



## Continuous Hydrothermal Flow Synthesis of $\text{LaCrO}_3$ in Supercritical Water and Its Application in Dual-Phase Oxygen Transport Membranes

Xu, Yu; Pirou, Stéven; Zielke, Philipp; Simonsen, Søren Bredmose; Norby, Poul; Hendriksen, Peter Vang; Kiebach, Ragnar

*Published in:*  
Industrial and Engineering Chemistry Research

*Link to article, DOI:*  
[10.1021/acs.iecr.7b04390](https://doi.org/10.1021/acs.iecr.7b04390)

*Publication date:*  
2018

*Document Version*  
Peer reviewed version

[Link back to DTU Orbit](#)

*Citation (APA):*  
Xu, Y., Pirou, S., Zielke, P., Simonsen, S. B., Norby, P., Hendriksen, P. V., & Kiebach, R. (2018). Continuous Hydrothermal Flow Synthesis of  $\text{LaCrO}_3$  in Supercritical Water and Its Application in Dual-Phase Oxygen Transport Membranes. *Industrial and Engineering Chemistry Research*, 57(6), 2123-2130.  
<https://doi.org/10.1021/acs.iecr.7b04390>

---

### General rights

Copyright and moral rights for the publications made accessible in the public portal are retained by the authors and/or other copyright owners and it is a condition of accessing publications that users recognise and abide by the legal requirements associated with these rights.

- Users may download and print one copy of any publication from the public portal for the purpose of private study or research.
- You may not further distribute the material or use it for any profit-making activity or commercial gain
- You may freely distribute the URL identifying the publication in the public portal

If you believe that this document breaches copyright please contact us providing details, and we will remove access to the work immediately and investigate your claim.

Article

## Continuous Hydrothermal Flow Synthesis of $\text{LaCrO}_3$ in Supercritical Water and Its Application in Dual-Phase Oxygen Transport Membranes

Yu Xu, Stéven Pirou, Philipp Zielke, Søren Bredmose Simonsen,  
Poul Norby, Peter Vang Hendriksen, and Ragnar Kiebach

*Ind. Eng. Chem. Res.*, **Just Accepted Manuscript** • DOI: 10.1021/acs.iecr.7b04390 • Publication Date (Web): 22 Jan 2018

Downloaded from <http://pubs.acs.org> on January 29, 2018

### Just Accepted

"Just Accepted" manuscripts have been peer-reviewed and accepted for publication. They are posted online prior to technical editing, formatting for publication and author proofing. The American Chemical Society provides "Just Accepted" as a free service to the research community to expedite the dissemination of scientific material as soon as possible after acceptance. "Just Accepted" manuscripts appear in full in PDF format accompanied by an HTML abstract. "Just Accepted" manuscripts have been fully peer reviewed, but should not be considered the official version of record. They are accessible to all readers and citable by the Digital Object Identifier (DOI®). "Just Accepted" is an optional service offered to authors. Therefore, the "Just Accepted" Web site may not include all articles that will be published in the journal. After a manuscript is technically edited and formatted, it will be removed from the "Just Accepted" Web site and published as an ASAP article. Note that technical editing may introduce minor changes to the manuscript text and/or graphics which could affect content, and all legal disclaimers and ethical guidelines that apply to the journal pertain. ACS cannot be held responsible for errors or consequences arising from the use of information contained in these "Just Accepted" manuscripts.



ACS Publications

# Continuous Hydrothermal Flow Synthesis of $\text{LaCrO}_3$ in Supercritical Water and Its Application in Dual-Phase Oxygen Transport Membranes

Yu Xu \*, Stéven Pirou, Philipp Zielke, Søren Bredmose Simonsen, Poul Norby, Peter Vang Hendriksen, Ragnar Kiebach

Department of Energy Conversion and Storage, Technical University of Denmark (Risø Campus), Frederiksborgvej 399, 4000 Roskilde, Denmark

\* Correspondence: Y. Xu, Tel.: +45 93511148, Fax: +45 46775688, Email: [yuax@dtu.dk](mailto:yuax@dtu.dk)

## Abstract

The continuous production of  $\text{LaCrO}_3$  particles (average edge size 639 nm, cube-shaped) by continuous hydrothermal flow synthesis using supercritical water is reported for the first time. By varying the reaction conditions, it was possible to suggest a reaction mechanism for the formation of this perovskite material. Moreover, dual-phase oxygen transport membranes were manufactured from the as-synthesized  $\text{LaCrO}_3$  particles and  $(\text{ZrO}_2)_{0.89}(\text{Y}_2\text{O}_3)_{0.01}(\text{Sc}_2\text{O}_3)_{0.10}$  (10Sc1YSZ), and oxygen permeation fluxes up to  $5 \times 10^{-8} \text{ mol cm}^{-2} \text{ s}^{-1}$  were measured on a 1-mm thick membrane.

**Keywords:** continuous flow synthesis; hydrothermal; supercritical water; perovskite; lanthanum chromite; oxygen transport membrane

## 1. Introduction

$\text{LaCrO}_3$  and based materials are known used as the electronic conducting phase in dual-phase oxygen transport membranes (OTMs).<sup>1</sup> In OTMs this class of materials is of interest, because of its chemical stability towards gas impurities (e.g.,  $\text{CO}_2$  and  $\text{SO}_2$ ) and reducing atmospheres.<sup>2</sup> OTMs are able to provide oxygen of high purity (>99 %) for a

wide range of applications, such as biomass gasification, oxy-fired cement production and oxy-fuel combustion.<sup>3</sup> In dual-phase OTMs, composites of an electronic-conductive material and an ionic-conductive material are used. Doped zirconia, for instance,  $(\text{Sc}_2\text{O}_3)_{0.10}(\text{Y}_2\text{O}_3)_{0.01}(\text{ZrO}_2)_{0.89}$  (10Sc1YSZ), is a very good ionic conductor.<sup>4,5</sup>

To implement  $\text{LaCrO}_3$  in the above-mentioned applications, a reliable, controllable and preferably scalable synthesis method is desired to prepare  $\text{LaCrO}_3$ -based oxide particles. Moreover, reducing the size of particles to the submicron- or nano-meter regime will facilitate sintering of  $\text{LaCrO}_3$ , which usually requires high temperatures ( $\sim 1,600^\circ\text{C}$  for  $\text{LaCrO}_3$  to get  $>90\%$  of the theoretical maximum density<sup>6</sup>). Similar to other lanthanide-transition metal complex oxides,  $\text{LaCrO}_3$ -based oxides can be prepared by conventional high-temperature (typically  $>1,000^\circ\text{C}$ ) solid-state reactions among stoichiometric amounts of simple oxides/carbonates.<sup>7</sup> Among the alternative synthesis approaches, the hydrothermal route is appealing because particles can be obtained directly without any post treatments. Moreover, hydrothermal synthesis is advantageous for controlling the composition, phase and size distribution of particles and is environmentally benign as water is used as the reaction medium. Hydrothermal synthesis of phase-pure  $\text{LaCrO}_3$  particles has been reported in literatures, reaction taking place in a batch-type reactor at a temperature higher than  $700^\circ\text{C}$  under a pressure of 100 MPa.<sup>8</sup> Later, it was brought to mild hydrothermal conditions<sup>9–14</sup> in which lower temperatures ( $260 - 425^\circ\text{C}$ ) and autogenous pressures were used.

Continuous hydrothermal flow synthesis (CHFS)<sup>15</sup> is employed in this work. Here, a continuous production of materials is achieved in a flow-type apparatus (CHFS reactor). This type of reactors usually contains a mixer, where a constantly fed room-temperature precursor flow is mixed with a flow of supercritical water ( $\text{scH}_2\text{O}$ ,  $T_C \geq 374^\circ\text{C}$ ,  $p_C \geq 22.1$

MPa) and is thereby rapidly heated to the (near-) supercritical state. Since the properties of water drastically change near the critical point, the solvent power of water and the hydrothermal reaction rate vary significantly.<sup>16</sup> A high degree of supersaturation is generated in a very short time and nucleation almost starts instantaneously upon mixing. Therefore, the scH<sub>2</sub>O provides an ideal reaction environment for hydrothermal synthesis particularly of nanomaterials. The preparation of several nanomaterials by CHFS has been reported on a laboratory scale, including oxides,<sup>17–19</sup> metals,<sup>20</sup> sulfides,<sup>21</sup> metal organic frame works (MOFs),<sup>22</sup> layered double hydroxides<sup>23</sup> and minerals,<sup>24,25</sup> and the upscaling ability of CHFS to an industrial scale has been shown for several compounds.<sup>26,27</sup> However, compared with the CHFS of simple oxides, there are rather few reports on the one-step continuous synthesis of complex lanthanide-transition metal oxides (La<sub>n+1</sub>Ni<sub>n</sub>O<sub>3n+1</sub> after post heat treatment,<sup>28</sup> La<sub>1-x</sub>Sr<sub>x</sub>MnO<sub>3</sub>,<sup>29</sup> and La<sub>2</sub>CuO<sub>4</sub><sup>30</sup> ).

In this work the synthesis of LaCrO<sub>3</sub> particles by CHFS in scH<sub>2</sub>O is reported for the first time, and a mechanism for the formation of the LaCrO<sub>3</sub> particles is suggested. The synthesized powders were used to manufacture a set of small planar OTMs. The powders were sintered with 10Sc1YSZ powders at a temperature as low as 1400 °C, and the resulting dense dual-phase membranes were characterized in terms of microstructure and oxygen permeability.

## 2. Experimental

### 2.1 Materials

The 0.1 mol L<sup>-1</sup> (combined La<sup>3+</sup> and Cr<sup>3+</sup> concentration) reactant solution was prepared by dissolving as-bought La(NO<sub>3</sub>)<sub>3</sub>•6H<sub>2</sub>O (0.05 mol L<sup>-1</sup>, Sigma Aldrich, ≥ 99.0%) and Cr(NO<sub>3</sub>)<sub>3</sub>•9H<sub>2</sub>O (0.05 mol L<sup>-1</sup>, Sigma Aldrich, ≥ 99.0%) in deionized H<sub>2</sub>O (DI H<sub>2</sub>O). KOH

solutions of various concentrations (0.5, 1, 2, 4 and 6 mol L<sup>-1</sup>) were prepared by dissolving the corresponding amounts of KOH pellets (Sigma Aldrich, ≥ 85%) in DI H<sub>2</sub>O. Commercial 10Sc1YSZ powder ((Sc<sub>2</sub>O<sub>3</sub>)<sub>0.10</sub>(Y<sub>2</sub>O<sub>3</sub>)<sub>0.01</sub>(ZrO<sub>2</sub>)<sub>0.89</sub>, Daiichi Kigenso Kagaku Kogyo Co. Ltd., Japan) was used as the ionic-conductive material for preparing the dual-phase 10Sc1YSZ – LaCrO<sub>3</sub> OTMs.

## 2.2 Preparation of LaCrO<sub>3</sub> by CHFS

The in-house developed two-stage CHFS reactor was used to conduct the syntheses. Details of the reactor can be found elsewhere.<sup>31</sup> In a synthesis process, a flow of DI H<sub>2</sub>O was heated and pressurized to the supercritical state by pumping it through a preheater (4 kW). Meanwhile, flows of the reactant solution and the KOH solution were separately pumped to the reactor and formed a pre-mixture flow at the room temperature prior to being heated by the scH<sub>2</sub>O flow at the first mixing stage. The outflow then passed through the second mixing stage and the re-heater (1.8 kW), and was rapidly cooled down to the room temperature by a water-cooled tube-in-tube heat exchanger. The products flow passed an in-line filter (Swagelok, 90-μm pore size) and was then depressurized to the atmospheric pressure by a backpressure regulator (Tescom, 26-1700 Series). The synthesized particles were harvested as slurries at the outlet of the reactor. MILROYAL metering pumps were used to feed all liquids to the reactor. The flow rates of pumps were calibrated with DI H<sub>2</sub>O before synthesis and the total flow rate was 65 mL min<sup>-1</sup>. Thermocouples inserted into the reactor were used to monitor the temperatures of flows. The pressure was controlled by the backpressure regulator at 28(±1) MPa throughout the entire synthesis. A summary of the experimental conditions (particles LC1 – LC5) with varying temperatures and pH values can be found (**Table S1**) in **SI**. The current employed reactor is made of 316 stainless steel,<sup>31</sup> but an Inconel compartment will be applied in

the future to ensure higher chemical resistance under the here applied syntheses conditions.<sup>12,14</sup>.

### 2.3 Preparation of 10Sc1YSZ – LaCrO<sub>3</sub> OTMs

Symmetrical membranes based on a dual-phase composite consisting of 10Sc1YSZ as the ionic conductor and LaCrO<sub>3</sub> as the electronic conductor were prepared and tested by oxygen permeation measurements. For the membranes, LaCrO<sub>3</sub> from sample LC5 was used because this was found to contain the purest LaCrO<sub>3</sub> as will be described in detail later. The commercial 10Sc1YSZ and the as-prepared LaCrO<sub>3</sub> (LC5) powders were blended in a 65 – 35 vol. % ratio. A milling process using an agate mortar was applied to mix the two powders homogeneously. Thereafter, 15 mm-diameter pellets were formed by die-pressing at 1,000 kg load and then isostatically pressed at 65,000 kg load. The dense membranes were obtained by sintering the green pellets at 1,400 °C for 6 h in air (heating and cooling ramps were both 100 °C h<sup>-1</sup>). The samples intended for the oxygen permeation measurement were polished down to 1-mm thickness, and an ink made from (La<sub>0.80</sub>Sr<sub>0.20</sub>)MnO<sub>3-δ</sub> – (Y<sub>2</sub>O<sub>3</sub>)<sub>0.08</sub>(ZrO<sub>2</sub>)<sub>0.92</sub> (LSM – YSZ, 50 – 50 vol. %) was applied by screen printing on both sides of the membranes to serve as oxygen redox catalyst. Prior to the measurement, the samples were heated to 980 °C for 2 h in air in order to sinter mildly the printed LSM – YSZ layers.

### 2.4 Characterization

Particles were separated from slurries using a centrifuge, then cleaned with DI H<sub>2</sub>O and dried at ambient conditions. Powder XRD patterns were obtained by using a Bruker Robot D8 diffractometer (Cu Kα 0.154 nm, 10 – 120° in stepsize 0.01°). Patterns were refined in the Rietveld method using the FullProf software suite.<sup>32</sup> Raman spectra of particles were

recorded using a Renishaw inVia Reflex confocal Raman microscope. A 532-nm laser and 50X microscope objective were employed. The presented spectrum was averaged and background-corrected. For the TEM characterization, particles were re-dispersed in ethanol and dripped onto a holey carbon film/Au grid. Bright field TEM (BF-TEM) imaging and selected area electron diffraction (SAED) were conducted by using a JEOL 3000F microscope (300 kV). Dark-field scanning transmission electron microscopy (DF-STEM) was carried out using the JEOL 3000F equipped with a STEM unit and a high angle annular dark field (HAADF) detector. The nominal probe size was 0.5 nm and the camera length was 12 cm. For compositional analysis, energy dispersive X-ray spectroscopy (EDS) was carried out using the equipped Oxford Instruments EDS detector and was processed by the INCA EDS analysis software (Oxford instruments). For the SEM characterization, particles dispersed on carbon tapes were brought to a Zeiss Merlin (10 kV). A high-efficiency secondary electron (HE-SE2) detector was used to record microscopy images. The size of particles was measured by the ImageJ software.

The sintered 10Sc1YSZ – LaCrO<sub>3</sub> pellet was cut, embedded in epoxy, polished and carbon coated for SEM (the Zeiss Merlin, 5 kV) investigations of the cross section. The HE-SE2 detector and ES-BSE (energy-selective backscattered electron) detector were used to record images simultaneously at each selected area. A membrane prior to the test was cut and polished for SEM investigations of the cross section by using a Hitachi Tabletop TM3000 (15 kV). The software ThreshAlyzer was used for image segmentation and statistic quantification of density. Membrane dimensions and LaCrO<sub>3</sub> grain sizes were measured by the ImageJ software.

## 2.5 Oxygen permeation measurements



Oxygen permeation measurements were conducted in an Oxygen Membrane Rig built at DTU Energy described elsewhere.<sup>33</sup>. The sample was placed in-between two alumina tubes in the center of a height-adjustable tube furnace. Thermocouples were inserted into the tubes and were in contact with the sample in order to monitor the temperature. Before the test, the sample was sealed to the tubes by tape-cast sodium aluminosilicate (NAS,<sup>34</sup>. Na<sub>2</sub>O 17.8 mol %, Al<sub>2</sub>O<sub>3</sub> 9.4 mol % and SiO<sub>2</sub> 72.8 mol%) glass gaskets with an inner diameter of 9 mm and a glass transition temperature of 515 °C.<sup>33</sup>. The side walls of the sample were also coated with the NAS paste to ensure that no oxygen entered from the sweep gas compartment outside of the tubes. The sample was heated to 940 °C in air and afterwards cooled to 750 °C to ensure a gas-tight seal. A gas chromatograph was connected to the outlet of the permeate side to quantify the oxygen leak into the permeate stream. Air was fed to the feed side with a constant flowrate of 100 mL<sub>N</sub> min<sup>-1</sup>, while N<sub>2</sub> as a carrier gas was fed to the inlet of the permeate side with various flowrates from 20 mL<sub>N</sub> min<sup>-1</sup> to 150 mL<sub>N</sub> min<sup>-1</sup>. The gas flow was controlled and monitored by a mass flow controller (Brooks).

### 3. Results and Discussion

#### 3.1 Continuous hydrothermal flow synthesis of LaCrO<sub>3</sub>

In the XRD pattern (**Fig. 1a**) of LC1, the diffraction peaks match well to those of the reference pattern of La(OH)<sub>3</sub> (ICSD *PDF* 01-075-1900, hexagonal structure). **Fig. 1b** presents a BF-TEM image of particles in LC1. Nanowires with a uniform diameter of around 22 nm and a length ranging from nanometers to submicrometers were observed. The high-resolution TEM image (**Fig. 1c**) shows that the nanowires were well crystallized. The measured interplanar spacing (3.1 Å) is consistent with the distance of the (101)

planes of a hexagonal  $\text{La}(\text{OH})_3$  crystal. Besides the  $\text{La}(\text{OH})_3$  nanowires, additional nanosized particulates with an irregular morphology can be found in **Fig. 1b** as agglomerates around the nanowires. The high-resolution TEM image of these irregular-shaped particles (**Fig. 1d**) does not show any periodic crystallographic features, indicating that these particles were amorphous and therefore did not create any diffraction peaks in the XRD pattern. EDS analysis suggested that the irregular-shaped particles were amorphous Cr compounds. Characterizations on LC2 particles showed similar results (**Fig. S1, Table S2** in SI). In conclusion,  $\text{LaCrO}_3$  was not formed under synthesis conditions used for LC1 or LC2. Instead, composites of well crystallized  $\text{La}(\text{OH})_3$  and amorphous Cr compounds were obtained.

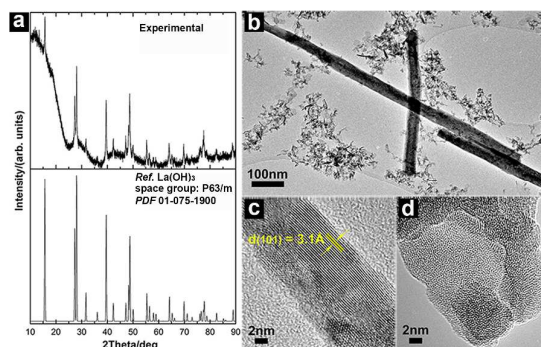


**Figure 1.** (a) XRD pattern and (b) BF-TEM image of LC1 particles; HR-TEM images of the nanowire (c) and of the irregular-shaped particles (d) observed in (b).

In principle, the presence of soluble and reactive hydrated complexes of both lanthanide cations  $\text{Ln}^{3+}$  and transition metal cations  $\text{Me}^{3+}$  in aqueous solutions is necessary to initiate the formation of  $\text{LnMeO}_3$ <sup>35</sup>. through the hydrothermal route. Aqueous  $\text{La}^{3+}$  would be readily subject to hydration after being mixed with a strong alkaline solution (KOH in this case), forming  $\text{La}(\text{OH})_3$ .  $\text{La}(\text{OH})_3$  has a nearly negligible solubility similar to other lanthanide trihydroxides<sup>35</sup>. and is very stable at an ambient temperature.<sup>36</sup>. However, the

solubility of  $\text{La}(\text{OH})_3$  increases with increasing the temperature. In addition,  $\text{La}(\text{OH})_3$  will dehydrate to  $\text{LaOOH}$ .  $\text{LaOOH}$  is more reactive and is more dissolved in water as a result of the reduced shielding of  $\text{La}^{3+}$  from the aqueous ligands.<sup>35</sup> Previous research<sup>37</sup> using high-temperature XRD showed that  $\text{La}(\text{OH})_3$  is stable below 420 °C while  $\text{LaOOH}$  is present at temperatures in-between 380 – 580 °C. It is therefore reasonable to assume that by mixing the nitrates solution and KOH solution in the tee-junction before the first mixer,  $\text{La}(\text{OH})_3$  was formed instantly in the precursor, which further crystallized in the form of nanowires when heated by the  $\text{scH}_2\text{O}$  (at the first mixer) due to the anisotropic crystal growth governed by its inherent crystal structure.<sup>38</sup> In comparison,  $\text{Cr}_2\text{O}_3$  is known for its amphoteric behavior. The solubility of  $\text{Cr}(\text{OH})_3$  is pronouncedly enhanced at increased pH values, and can be increased by i) using an alkali solution of a higher concentration, and ii) increasing the temperature.<sup>35,39</sup> It is known that in a typical hydrothermal process, the crystallization of an oxide usually follows a ‘dissolution-precipitation’ mechanism.<sup>11</sup> The presence of amorphous Cr compounds possibly indicates that the solubility of Cr-hydrated complexes was rather low at the applied synthesis conditions of LC1 and LC2. In summary, due to the absence of i)  $\text{LaOOH}$  (depending on the reaction temperature) and/or ii) soluble Cr-hydrated complexes, i.e.  $[\text{Cr}(\text{OH})_4]^-$  in alkaline aqueous solutions<sup>39</sup> (depending on the concentration of KOH),  $\text{LaCrO}_3$  was not formed.

In comparison,  $\text{LaCrO}_3$  was obtained in the LC5 particles (**Fig. 2**). Rietveld refinement (**Fig. 2a**) of the diffraction pattern showed that only  $\text{LaCrO}_3$  was present in LC5. Shown in the SEM image (**Fig. 2b**) and the BF-TEM image (**Fig. 2c**), the  $\text{LaCrO}_3$  particles displayed a cube-like morphology. Measuring the edge size of 10 particles gave an average value of  $639 \pm 47$  nm. **Fig. 2d** presents an exemplary SAED pattern of a  $\text{LaCrO}_3$  particle, in which all diffraction dots are assigned to specific planes of an orthorhombic  $\text{LaCrO}_3$  crystal along

the zone axis [011], indicating that particles were single crystals. The phase purity of the LC5 particles was further analyzed by Raman spectroscopy (**Fig. 2e**). All indexed Raman peaks below  $600\text{ cm}^{-1}$  were assigned to modes of  $\text{LaCrO}_3$  of a *Pnma* orthorhombic structure.<sup>40–42</sup> The DF-STEM image (**Fig. 2f**) of a  $\text{LaCrO}_3$  particle also reveals a cube-like shape. STEM-EDS maps of La and Cr are presented in **Fig. 2g** and **2h** respectively. The similar distribution of the two elements in the particle suggests a homogeneous elemental composition.

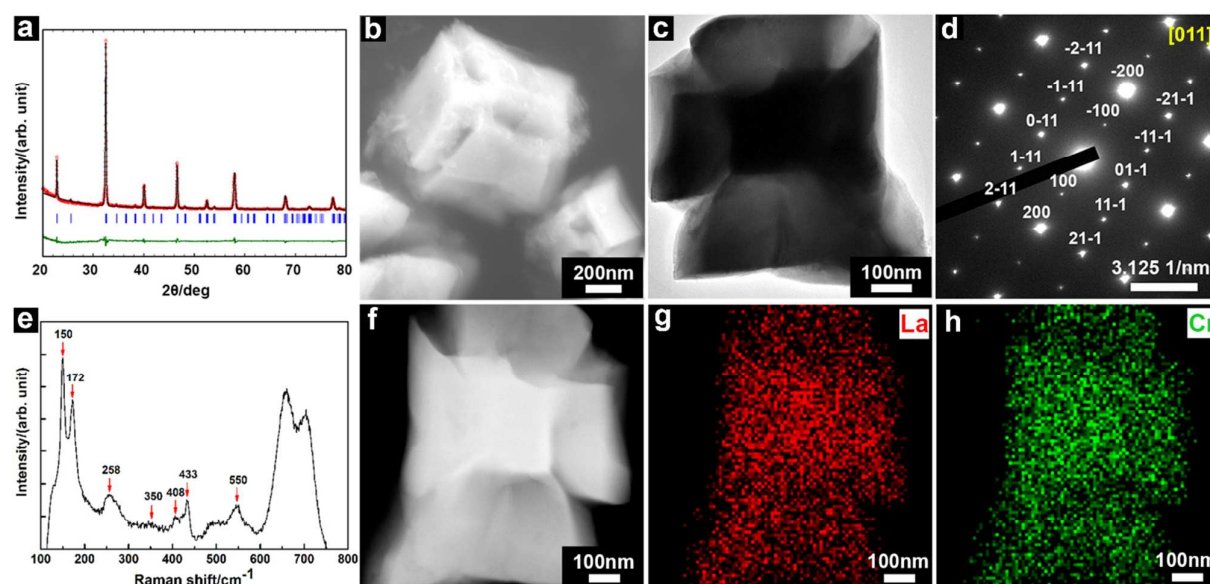


**Figure 2.** (a) Rietveld refinement of the powder XRD of the LC5 particles; the observed pattern (red circles), the calculated pattern (black line), difference profiles between the observed and the calculated pattern (bottom green line) and the Bragg reflection positions (blue vertical bars) of an orthorhombic  $\text{LaCrO}_3$  crystal; (b) SEM image of the LC5 particles; (c) BF-TEM image of a  $\text{LaCrO}_3$  particle; (d) SAED of a  $\text{LaCrO}_3$  particle; (e) Raman spectrum of the LC5 particles; (f) DF-STEM image of a  $\text{LaCrO}_3$  particle and STEM-EDS element mapping of the particle, X-ray photons of La  $\text{La}$  (g) and Cr  $\text{K}\alpha$  (h) are presented.

$\text{LaCrO}_3$  was found as the main phase in the LC3 and LC4 particles, while secondary phases including crystallized  $\text{La}(\text{OH})_3$  and amorphous Cr compounds were found as well (**Fig. S5** in **SI**). Suggested by the results, it is likely that  $\text{LaOOH}$  was formed during the

syntheses of LC3, LC4 and LC5, due to the increased reaction temperature (325 – 410 °C), which is in the range (380 – 580 °C)<sup>37</sup>. in which LaOOH should be present. For comparison, the reaction temperature in the synthesis of LC1 and LC2 was 285 – 385 °C. Moreover, the dehydration rate of La(OH)<sub>3</sub> to LaOOH is also largely dependent on the temperature. An estimation of the dehydration rate<sup>43</sup>. (see details in **SI**) shows that the rate in the syntheses of LC3, LC4 and LC5 was nearly two times the rate in the LC1 and LC2 cases. Given the short mean residence time<sup>44</sup>. (34 – 40 s) (see details in **SI**) of the CHFS process, a fast conversion from La(OH)<sub>3</sub> to LaOOH is important for the yield of LaCrO<sub>3</sub>. As described in detail above, the KOH concentration affects the concentration of the soluble [Cr(OH)<sub>4</sub>]<sup>-</sup>. Therefore, one can expect that for LC3 and LC4 synthesized with KOH solutions of lower concentrations than in LC5 (2 mol L<sup>-1</sup> and 4 mol L<sup>-1</sup> respectively), the Cr<sup>3+</sup> was possibly not fully converted. Some LaOOH was therefore left unreacted, since the molar ratio of La to Cr was 1 : 1 in the precursor. After the reaction, when the temperature decreased, the LaOOH was converted to La(OH)<sub>3</sub>, while the undissolved Cr compounds formed an amorphous phase (no ‘dissolution – precipitation’ process<sup>11</sup>). On the other hand, the use of a KOH solution of 6 mol L<sup>-1</sup> ( $n[\text{OH}^-] / n[\text{Me}^{3+}] = 60$ ) as used for LC5 enabled the formation of [Cr(OH)<sub>4</sub>]<sup>-</sup> which reacted with the LaOOH to form LaCrO<sub>3</sub> particles. The formation mechanism of LaCrO<sub>3</sub> was accordingly proposed (**Fig. 3**).

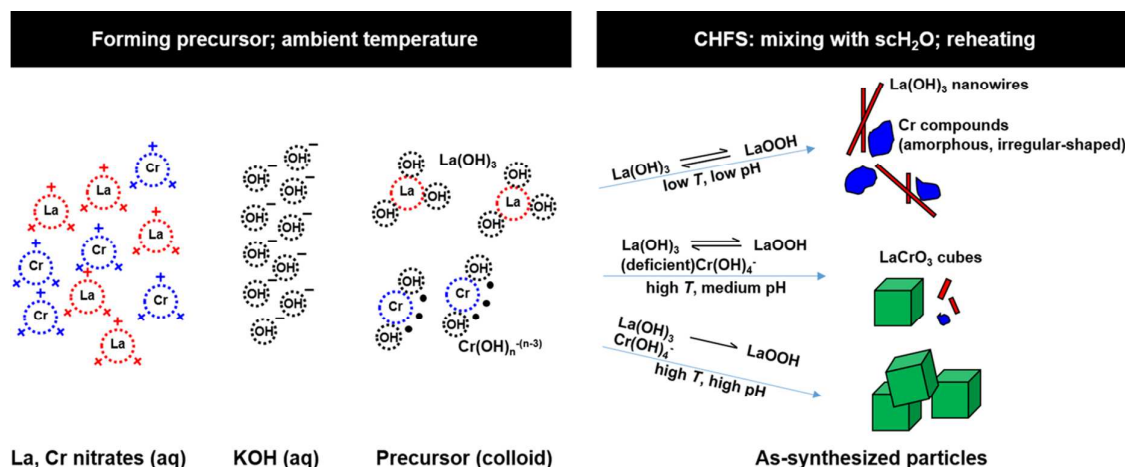


**Figure 3.** Mechanism suggested for the formation of  $\text{LaCrO}_3$ .

### 3.2 10Sc1YSZ – $\text{LaCrO}_3$ dual-phase oxygen transport membranes

Dual-phase oxygen transport membranes consisting of a stable ionic conductor and a stable electronic conductor can be an alternative to single-phase membranes composed of mixed-ionic-electronic conductive materials, and are capable of providing a high oxygen flux while being chemically stable.

In this study, planar dual-phase membranes were made from as-synthesized  $\text{LaCrO}_3$  particles (LC5, phase-pure) and 10Sc1YSZ. 10Sc1YSZ was chosen as the ionic conductive phase in the membranes, because of its known good ionic conductivity and chemical stability.<sup>5</sup>

#### 3.2.1 Microstructure of dual-phase 10Sc1YSZ – $\text{LaCrO}_3$ membranes

The microstructure of the sintered 10Sc1YSZ –  $\text{LaCrO}_3$  membrane is shown in **Fig. 4**. In general, the composite material was dense, and only closed porosity could be observed (**Fig. 4a**). A statistic quantification of seven SEM images gave an average relative density of 88 vol. %. It is worth mentioning that this is a rather high density for sintering  $\text{LaCrO}_3$ -based materials, indicating that the synthesized  $\text{LaCrO}_3$  particles displayed a good



sinterability.<sup>45</sup> Distinguishable by the contrast, the distribution of  $\text{LaCrO}_3$  (light grey) and 10Sc1YSZ (dark grey) is presented in **Fig. 4b**. Both phases were evenly distributed assuring possible conduction paths for electrons and oxygen ions, which is important for an application as oxygen transport membrane. The average grain size of  $\text{LaCrO}_3$  was  $922 \pm 125$  nm, indicating that  $\text{LaCrO}_3$  grew during the sintering process (for reference, the size of as-synthesized  $\text{LaCrO}_3$  particles was  $639 \pm 47$  nm).

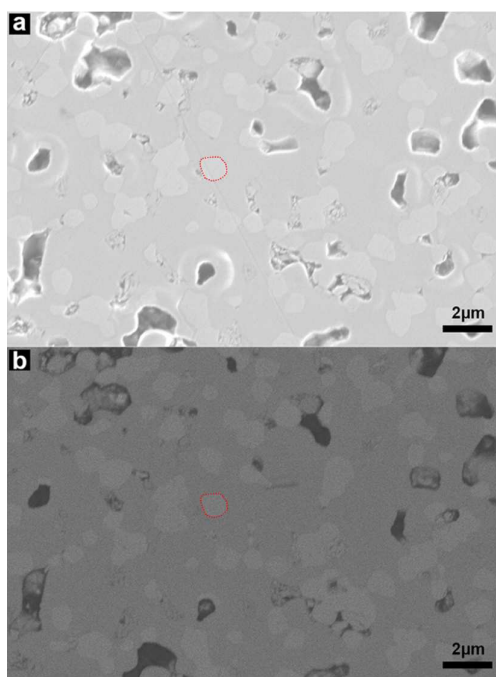


**Figure 4.** Microstructure of the sintered 10Sc1YSZ –  $\text{LaCrO}_3$  membranes, presented by HE-SE2 (**a**) and ES-BSE (**b**); a  $\text{LaCrO}_3$  grain is highlighted by red dashed lines.

### 3.2.2 Oxygen permeability

Oxygen permeation measurements were carried out on a 1 mm thick self-standing 10Sc1YSZ –  $\text{LaCrO}_3$  (65 – 35 vol. %) membrane. **Fig. 5** presents the microstructure of the polished cross section of the symmetrical membrane with catalyst layers for oxygen permeation measurement. The screen-printed LSM – YSZ (50 – 50 vol. %) layers after

heat treatment at 980 °C were 13 – 14  $\mu\text{m}$  thick, and were well attached to the 10Sc1YSZ –  $\text{LaCrO}_3$  (65 – 35 vol. %, 960  $\mu\text{m}$ ).

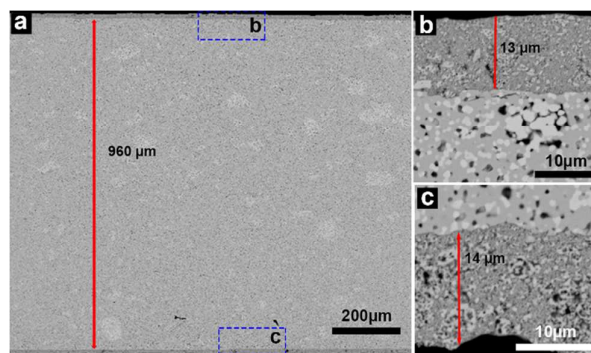


**Figure 5.** SE2 micrographs of the cross section of the sample for oxygen permeation measurement test.

**Fig. 6a** presents the oxygen permeation flux across the membrane as a function of the natural logarithm of the ratio between the oxygen partial pressures in the feed and permeate side gases (equivalent to the driving force). Shown by the solid lines, the experimentally measured flux across the membrane scaled proportionally with the driving force, proving that no gas leak occurred during the oxygen permeation measurement. Moreover, as the temperature increased, the flux increased for all oxygen partial pressure ratios. Among all measurement conditions, the highest flux corresponded to  $5 \times 10^{-8} \text{ mol cm}^{-2} \text{ s}^{-1}$  or  $0.066 \text{ mL}_N \text{ cm}^{-2} \text{ s}^{-1}$  (air/ $\text{N}_2$ , 900 °C).

In the case of dense self-supported membranes, the dominating rate-limiting process that governs the oxygen flux can either be the diffusion of oxygen ions or electrons within the bulk of membranes or the kinetics of oxygen redox reactions at the surfaces of membranes. Here, the oxygen flux scaled in proportion to the driving force across the membrane, indicating that the main limiting factor of the oxygen permeation is the bulk diffusion. The diffusion-limited oxygen flux can be calculated by the *Wagner Equation*.<sup>1</sup> The calculation of the expected oxygen permeation flux was performed for the membrane,



taking account of the volume fractions and bulk conductivities of 10Sc1YSZ and LaCrO<sub>3</sub> obtained from references.<sup>4,46</sup> Details of calculations can be found in **SI**. Results are presented in **Fig. 6a** by the hollow symbols and dashed lines. At all temperatures, the calculated values of the oxygen flux lie above the experimental values ( $J_{O_2,Cal} / J_{O_2,Exp} = 1.3 - 2.4$ ), suggesting that other factors also affected the measured oxygen flux. One of them can be the tortuosity factor  $\tau$  that is the partial 'blocking' of electron/ion paths in the membrane resulting in more tortuous paths for electrons/ions (i.e., a larger effective thickness of the membrane).<sup>33</sup> By integrating a tortuosity factor  $\tau$  (1.3 – 2.4) into the calculations, the corrected expected oxygen flux would approach the measured flux.

The Arrhenius-type plots of the oxygen flux of the membrane versus the temperature are shown in **Fig. 6b**. The apparent activation energy  $E_{a, flux}$  for the oxygen permeation of the membrane was derived at different driving forces, with an average value of 12.6 kJ mol<sup>-1</sup>. LaCrO<sub>3</sub> displays a thermally activated behavior of the electrical conductivity with an activation energy  $E_{a, electric}$  of 16.0 kJ mol<sup>-1</sup> (298 – 1473 K, in air),<sup>46</sup> while the temperature-dependent ionic conductivity of 10Sc1YSZ is characterized by an activation energy  $E_{a, ionic}$  of 62.7 kJ mol<sup>-1</sup> (973 – 1273 K, in air).<sup>4</sup>  $E_{a, flux}$  is closer to  $E_{a, electric}$  than to  $E_{a, ionic}$ , suggesting that the oxygen flux of the membrane is limited by the electric conductivity of LaCrO<sub>3</sub>. Given that doping LaCrO<sub>3</sub> oxide significantly increases the conductivity,<sup>46</sup> further improvements of the oxygen permeability of the membrane can be expected.

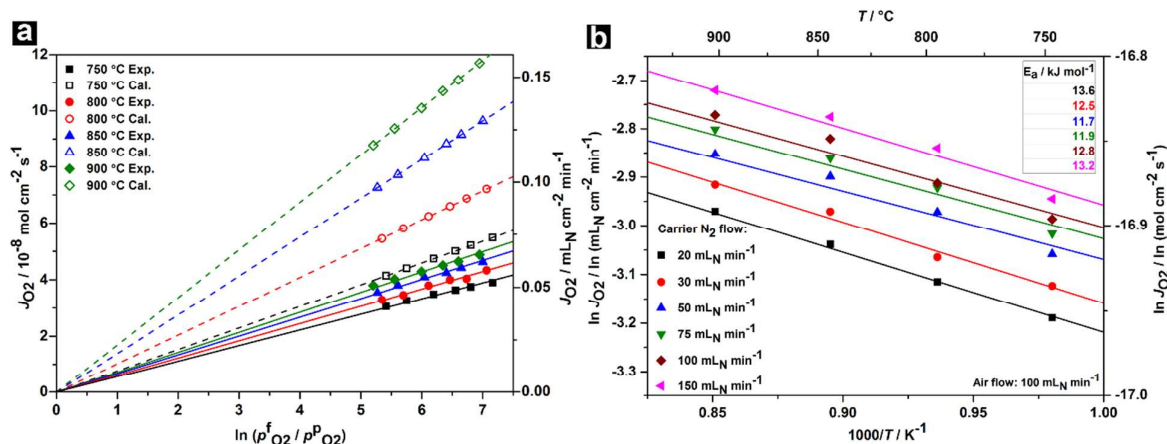


**Figure 6.** (a) Oxygen permeation flux  $J_{O_2}$  across a 1 mm-thick 10Sc1YSZ – LaCrO<sub>3</sub> (65 – 35 vol. %) membrane as a function of the driving force, i.e. log of the ratio between oxygen partial pressures in the feed ( $p_{O_2}^f$ , 0.21 atm) and permeate ( $p_{O_2}^p$ ) side gases. The air flowrate at the feed side was constant at 100  $\text{mL}_N \text{ min}^{-1}$ , while  $N_2$  of various flowrates (20, 30, 50, 75, 100 and 150  $\text{mL}_N \text{ min}^{-1}$ ) was fed to the inlet of the permeate side. The solid symbols describe the experimental (Exp.) values while the corresponding hollow symbols describe the calculated (Cal.) values. (b) Arrhenius plot of the oxygen permeation flux measured under air. The lines describe the best linear fit to the experimental data.

#### 4. Conclusion

In summary, LaCrO<sub>3</sub> sub-micron particles (cube-shaped, 639 nm in edge size) were prepared by continuous hydrothermal flow synthesis (CHFS) in supercritical water. A continuous production of phase-pure LaCrO<sub>3</sub> particles was achieved for the first time, at 410 °C and 28 MPa with a reaction time as short as 34 s. The as-synthesized LaCrO<sub>3</sub> particles were further used to prepare 10Sc1YSZ – LaCrO<sub>3</sub> dual-phase oxygen transport membranes with ~90 vol. % density after sintering at 1400 °C. Oxygen permeation fluxes of up to  $5 \times 10^{-8} \text{ mol cm}^{-2} \text{ s}^{-1}$  were obtained with a 1-mm thick membrane tested in air/ $N_2$  at 900 °C. Given that CHFS is relatively easy to be up-scaled, a rapid, large-scale production of fine LaCrO<sub>3</sub> particles can be achieved by CHFS. Moreover, using doped LaCrO<sub>3</sub>

(prepared by CHFS) with a higher electrical conductivity compared to the undoped material applied here is expected to improve the performance.

## Acknowledgement

The authors appreciate the *Danish Council for Independent Research (DFF)* for the funding within the project '*ProEco*' (Project No. DFF 1335-00138). The authors also thank Peter Stanley Jørgensen ([psjq@dtu.dk](mailto:psjq@dtu.dk), DTU Energy) for developing the *ThreshAlyzer* for image analysis.

Supporting Information. \*\*Comprehensive details on the experimental conditions and characterizations of particles LC2 to LC5; Estimations of the  $\text{La}(\text{OH})_3$  dehydration rate and the residence time of CHFS; Comprehensive characterization details of the membrane; Calculation of the expected oxygen permeation flux.\*\*

## References

- (1) Gupta, S.; Mahapatra, M. K.; Singh, P. Lanthanum Chromite Based Perovskites for Oxygen Transport Membrane. *Mater. Sci. Eng. R Reports* **2015**, *90*, 1–36.
- (2) Luo, Y.; Liu, T.; Gao, J.; Chen, C.  $\text{Zr}_{0.84}\text{Y}_{0.16}\text{O}_{1.92}-\text{La}_{0.8}\text{Sr}_{0.2}\text{Cr}_{0.5}\text{Fe}_{0.5}\text{O}_{3-\delta}$  Composite Membrane for  $\text{CO}_2$  Decomposition. *Mater. Lett.* **2012**, *86*, 5–8.
- (3) Puig-Arnavat, M.; Soprani, S.; Søgaaard, M.; Engelbrecht, K.; Ahrenfeldt, J.; Henriksen, U. B.; Hendriksen, P. V. Integration of Mixed Conducting Membranes in an Oxygen–steam Biomass Gasification Process. *RSC Adv.* **2013**, *3* (43), 20843–20854.
- (4) Irvine, J. T. S.; Dobson, J. W. L.; Politova, T.; Martín, S. G.; Shenouda, A. Co-Doping of Scandia-Zirconia Electrolytes for SOFCs. *Faraday Discuss.* **2007**, *134*, 41–49.
- (5) Pirou, S.; Gurauskis, J.; Gil, V.; Søgaaard, M.; Hendriksen, P. V.; Kaiser, A.; Ovtar, S.; Kiebach, R. Oxygen Permeation Flux through  $10\text{Sc}1\text{YSZ}-\text{MnCo}2\text{O}_4$  Asymmetric

- Membranes Prepared by Two-Step Sintering. *Fuel Process. Technol.* **2016**, *152*, 192–199.
- (6) Azegami, K.; Yoshinaka, M.; Hirota, K.; Yamaguchi, O. Formation and Sintering of LaCrO<sub>3</sub> Prepared by the Hydrazine Method. *Mater. Res. Bull.* **1998**, *33* (2), 341–348.
- (7) Fu, Y. P.; Wang, H. C.; Weng, C. S.; Hu, S. H.; Liu, Y. C. Characterizations of Fe Doping on B-Site of (La<sub>0.8</sub>Ca<sub>0.2</sub>)(Cr<sub>0.9</sub>Co<sub>0.1</sub>)O<sub>3-δ</sub> Interconnect Materials for SOFCs. *J. Am. Ceram. Soc.* **2015**, *98* (8), 2561–2569.
- (8) Yoshimura, M.; Song, S. T.; Sōmiya, S. Synthesis of LaCrO<sub>3</sub> under Hydrothermal Conditions. In *Hydrothermal Reactions for Materials Science and Engineering: An Overview of Research in Japan*; Sōmiya, S., Ed.; Springer Netherlands: Dordrecht, 1989; pp 284–288.
- (9) Zheng, W.; Pang, W.; Meng, G.; Peng, D. Hydrothermal Synthesis and Characterization of LaCrO<sub>3</sub>. *J. Mater. Chem.* **1999**, No. 9, 2833–2836.
- (10) Wang, S.; Huang, K.; Hou, C.; Yuan, L.; Wu, X.; Lu, D. Low Temperature Hydrothermal Synthesis, Structure and Magnetic Properties of RECrO<sub>3</sub> (RE = La, Pr, Nd, Sm). *Dalt. Trans.* **2015**, *44* (39), 17201–17208.
- (11) Rivas-Vázquez, L. P.; Rendón-Angeles, J. C.; Rodríguez-Galicia, J. L.; Gutiérrez-Chavarria, C. A.; Zhu, K. J.; Yanagisawa, K. Preparation of Calcium Doped LaCrO<sub>3</sub> Fine Powders by Hydrothermal Method and Its Sintering. *J. Eur. Ceram. Soc.* **2006**, *26* (1–2), 81–88.
- (12) Sardar, K.; Lees, M. R.; Kashtiban, R. J.; Sloan, J.; Walton, R. I. Direct Hydrothermal Synthesis and Physical Properties of Rare-Earth and Yttrium Orthochromite Perovskites. *Chem. Mater.* **2011**, *23* (1), 48–56.
- (13) Girish, H.-N.; Shao, G.-Q.; Basavalingu, B. Well-Monocrystallized LaCrO<sub>3</sub> Particles from a LaCrO<sub>4</sub> Precursor by Supercritical Hydrothermal Technique. *RSC Adv.* **2016**, *6* (83), 79763–79767.
- (14) Daniels, L. M.; Weber, M. C.; Lees, M. R.; Guennou, M.; Kashtiban, R. J.; Sloan, J.; Kreisel, J.; Walton, R. I. Structures and Magnetism of the Rare-Earth Orthochromite Perovskite Solid Solution La<sub>x</sub>Sm<sub>1-x</sub>CrO<sub>3</sub>. *Inorg. Chem.* **2013**, *52* (20), 12161–12169.
- (15) Adschiri, T.; Kanazawa, K.; Arai, K. Rapid and Continuous Hydrothermal Crystallization of Metal Oxide Particles in Supercritical Water. *J. Am. Ceram. Soc.* **1992**, *22* (196504), 1019–1022.

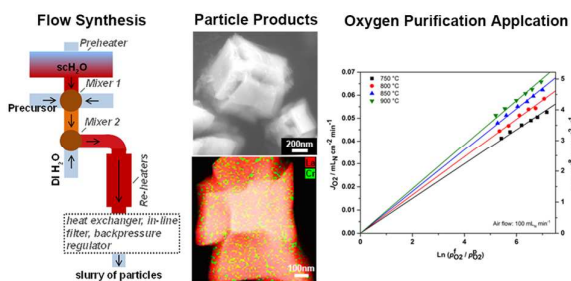
- (16) Adschiri, T.; Hakuta, Y.; Arai, K. Hydrothermal Synthesis of Metal Oxide Fine Particles at Supercritical Conditions. *Ind. Eng. Chem. Res.* **2000**, 39 (12), 4901–4907.
- (17) Nugroho, A.; Kim, J. Effect of KOH on the Continuous Synthesis of Cobalt Oxide and Manganese Oxide Nanoparticles in Supercritical Water. *J. Ind. Eng. Chem.* **2014**, 20 (6), 4443–4446.
- (18) Slostowski, C.; Marre, S.; Bassat, J.-M.; Aymonier, C. Synthesis of Cerium Oxide-Based Nanostructures in near- and Supercritical Fluids. *J. Supercrit. Fluids* **2013**, 84, 89–97.
- (19) Shen, Y.; Eltzholtz, J. R.; Iversen, B. B. Controlling Size, Crystallinity, and Electrochemical Performance of Li<sub>4</sub>Ti<sub>5</sub>O<sub>12</sub> Nanocrystals. *Chem. Mater.* **2013**, 25, 5023–5030.
- (20) Kubota, S.; Morioka, T.; Takesue, M.; Hayashi, H.; Watanabe, M.; Jr. Smith, R. L. Continuous Supercritical Hydrothermal Synthesis of Dispersible Zero-Valent Copper Nanoparticles for Ink Applications in Printed Electronics. *J. Supercrit. Fluids* **2014**, 86, 33–40.
- (21) Dunne, P. W.; Starkey, C. L.; Gimeno-Fabra, M.; Lester, E. H. The Rapid Size- and Shape-Controlled Continuous Hydrothermal Synthesis of Metal Sulphide Nanomaterials. *Nanoscale* **2014**, 6 (4), 2406–2418.
- (22) Munn, A. S.; Dunne, P. W.; Tang, S. V. Y.; Lester, E. H. Large-Scale Continuous Hydrothermal Production and Activation of ZIF-8. *Chem. Commun.* **2015**, 51, 12811–12814.
- (23) Pascu, O.; Marre, S.; Cacciuttolo, B.; Ali, G.; Hecquet, L.; Pucheault, M.; Prevot, V.; Aymonier, C. Instant One-Pot Preparation of Functional Layered Double Hydroxides (LDHs) via a Continuous Hydrothermal Approach. *ChemNanoMat* **2017**, 3 (9), 614–619.
- (24) Dumas, A.; Claverie, M.; Slostowski, C.; Aubert, G.; Careme, C.; Le Roux, C.; Micoud, P.; Martin, F.; Aymonier, C. Fast-Geomimicking Using Chemistry in Supercritical Water. *Angew. Chemie - Int. Ed.* **2016**, 55 (34), 9868–9871.
- (25) Diez-Garcia, M.; Gaitero, J. J.; Dolado, J. S.; Aymonier, C. Ultra-Fast Supercritical Hydrothermal Synthesis of Tobermorite under Thermodynamically Metastable Conditions. *Angew. Chemie - Int. Ed.* **2017**, 56 (12), 3162–3167.
- (26) Adschiri, T.; Lee, Y.-W.; Goto, M.; Takami, S. Green Materials Synthesis with Supercritical Water. *Green Chem.* **2011**, 13 (6), 1380–1390.

- (27) Gruar, R. I.; Tighe, C. J.; Darr, J. A. Scaling-up a Confined Jet Reactor for the Continuous Hydrothermal Manufacture of Nanomaterials. *Ind. Eng. Chem. Res.* **2013**, 52 (15), 5270–5281.
- (28) Weng, X.; Boldrin, P.; Abrahams, I.; Skinner, S. J.; Darr, J. A. Direct Syntheses of Mixed Ion and Electronic Conductors  $\text{La}_4\text{Ni}_3\text{O}_{10}$  and  $\text{La}_3\text{Ni}_2\text{O}_7$  from Nanosized Coprecipitates. *Chem. Mater.* **2007**, 19 (6), 4382–4384.
- (29) Islam, N. M.; Noguchi, T.; Hakuta, Y.; Hayashi, H. Hydrothermal Synthesis of Strontium Doped Lanthanum Manganite Nanoparticles by a Supercritical Flow Reaction System. *Nanosci. Nanotechnol. Lett.* **2011**, 3 (3), 324–327.
- (30) Galkin, A. A.; Kostyuk, B. G.; Lunin, V. V.; Poliakov, M. Continuous Reactions in Supercritical Water: A New Route to  $\text{La}_2\text{CuO}_4$  with a High Surface Area and Enhanced Oxygen Mobility. *Angew. Chemie Int. Ed.* **2000**, 39 (15), 2738–2740.
- (31) Zielke, P.; Xu, Y.; Simonsen, S. B.; Norby, P.; Kiebach, R. Simulation, Design and Proof-of-Concept of a Two-Stage Continuous Hydrothermal Flow Synthesis Reactor for Synthesis of Functionalized Nano-Sized Inorganic Composite Materials. *J. Supercrit. Fluids* **2016**, 117, 1–12.
- (32) Rodríguez-Carvajal, J. Recent Advances in Magnetic Structure Determination by Neutron Powder Diffraction. *Phys. B Condens. Matter* **1993**, 192 (1), 55–69.
- (33) Samson, A. J.; Søgaard, M.; Hendriksen, P. V. (Ce,Gd) $\text{O}_2$ - $\delta$ -Based Dual Phase Membranes for Oxygen Separation. *J. Memb. Sci.* **2014**, 470, 178–188.
- (34) Nielsen, K. A.; Solvang, M.; Nielsen, S. B. L.; Dinesen, A. R.; Beeaff, D.; Larsen, P. H. Glass Composite Seals for SOFC Application. *J. Eur. Ceram. Soc.* **2007**, 27 (2–3), 1817–1822.
- (35) Stamper, E. S.; Sheets, W. C.; Prellier, W.; Marks, T. J.; Poeppelmeier, K. R. Hydrothermal Synthesis of  $\text{LnMnO}_3$  (Ln = Ho–Lu and Y): Exploiting Amphoterism in Late Rare-Earth Oxides. *J. Mater. Chem.* **2009**, 19, 4375–4381.
- (36) Fleming, P.; Farrell, R. A.; Holmes, J. D.; Morris, M. A. The Rapid Formation of  $\text{La}(\text{OH})_3$  from  $\text{La}_2\text{O}_3$  Powders on Exposure to Water Vapor. *J. Am. Ceram. Soc.* **2010**, 93 (4), 1187–1194.
- (37) Füglein, E.; Walter, D. Thermal Analysis of Lanthanum Hydroxide. *J. Therm. Anal. Calorim.* **2012**, 110 (1), 199–202.
- (38) Feng, J.; Li, X.; Wang, M.; Zheng, X.; Bai, J.; Wang, L.; Peng, Y. One-Pot, Template-Free Synthesis of Hydrophobic Single-Crystalline  $\text{La}(\text{OH})_3$  Nanowires with Tunable Size and Their d0 Ferromagnetic Properties. *RSC Adv.* **2015**, 5 (21), 16093–16100.



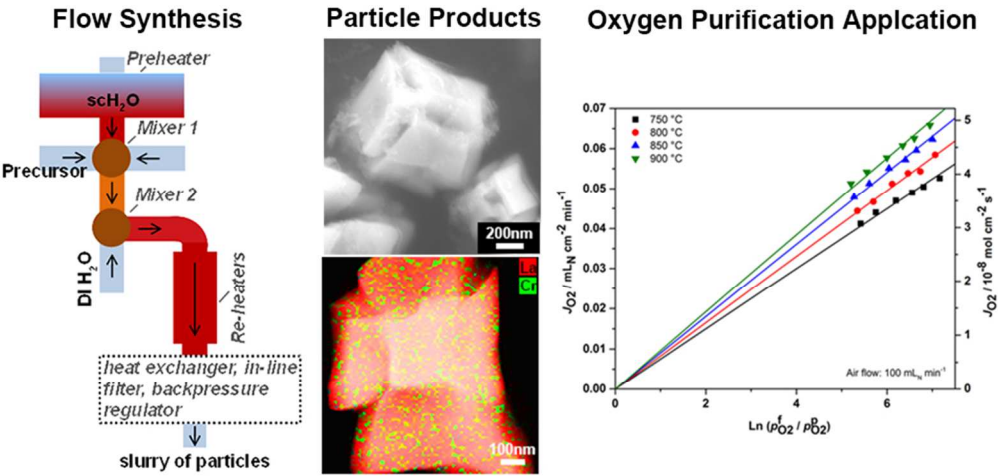
- (39) Brown, P. L.; Ekberg, C. First Transition Series Metals. In *Hydrolysis of Metal Ions*; Brown, P. L., Ekberg, C., Eds.; Wiley-VCH Verlag GmbH & Co. KGaA: Weinheim, Germany, 2016; pp 499–716.
- (40) Iliev, M. N.; Litvinchuk, A. P.; Hadjiev, V. G.; Wang, Y. Q.; Cmaidalka, J.; Meng, R. L.; Sun, Y. Y.; Kolev, N.; Abrashev, M. V. Raman Spectroscopy of Low-Temperature (Pnma) and High-Temperature (R-3c) Phases of LaCrO<sub>3</sub>. *Phys. Rev. B* **2006**, *74*, 214301 1-7.
- (41) Weber, M. C.; Kreisel, J.; Thomas, P. A.; Newton, M.; Sardar, K.; Walton, R. I. Phonon Raman Scattering of RCrO<sub>3</sub> Perovskites (R=Y, La, Pr, Sm, Gd, Dy, Ho, Yb, Lu). *Phys. Rev. B* **2012**, *85*, 054303 1-9.
- (42) Tompsett, G. A.; Sammes, N. M. Characterisation of the SOFC Material, LaCrO<sub>3</sub>, Using Vibrational Spectroscopy. *J. Power Sources* **2004**, *130*, 1–7.
- (43) Neumann, A.; Walter, D. The Thermal Transformation from Lanthanum Hydroxide to Lanthanum Hydroxide Oxide. *Thermochim. Acta* **2006**, *445* (2), 200–204.
- (44) Hakuta, Y.; Ura, H.; Hayashi, H.; Arai, K. Continuous Production of BaTiO<sub>3</sub> Nanoparticles by Hydrothermal Synthesis. *Ind. Eng. Chem. Res.* **2005**, *44* (4), 840–846.
- (45) Rivas-Vázquez, L. P.; Rendón-Angeles, J. C.; Rodríguez-Galicia, J. L.; Zhu, K.; Yanagisawa, K. Hydrothermal Synthesis and Sintering of Lanthanum Chromite Powders Doped with Calcium. *Solid State Ionics* **2004**, *172*, 389–392.
- (46) Bonet, A.; To Baben, M.; Travitzky, N.; Greil, P. High-Temperature Electrical Conductivity of LaCr<sub>1-x</sub>CoxO<sub>3</sub> Ceramics. *J. Am. Ceram. Soc.* **2016**, *99*, 917–921.

## TOC





1  
2  
3  
4  
5  
6  
7  
8  
9  
10  
11  
12  
13  
14  
15  
16  
17  
18  
19  
20  
21  
22  
23  
24  
25  
26  
27  
28  
29  
30  
31  
32  
33  
34  
35  
36  
37  
38  
39  
40  
41  
42  
43  
44  
45  
46  
47  
48  
49  
50  
51  
52  
53  
54  
55  
56  
57  
58  
59  
60



TOC

80x38mm (300 x 300 DPI)

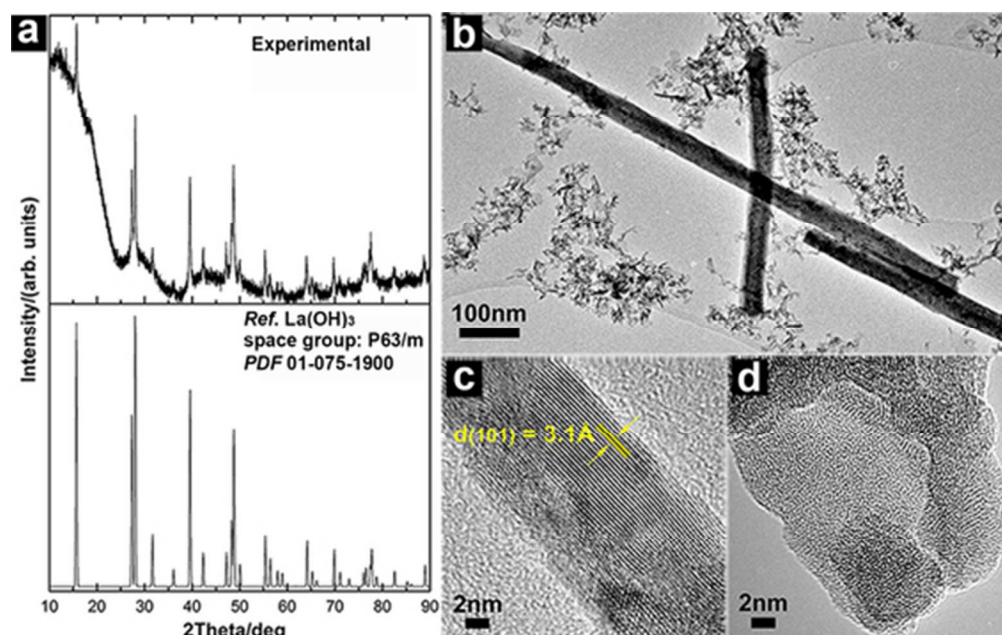


Figure 1. (a) XRD pattern and (b) BF-TEM image of LC1 particles; HR-TEM images of the nanowire (c) and of the irregular-shaped particles (d) observed in (b).

47x30mm (300 x 300 DPI)

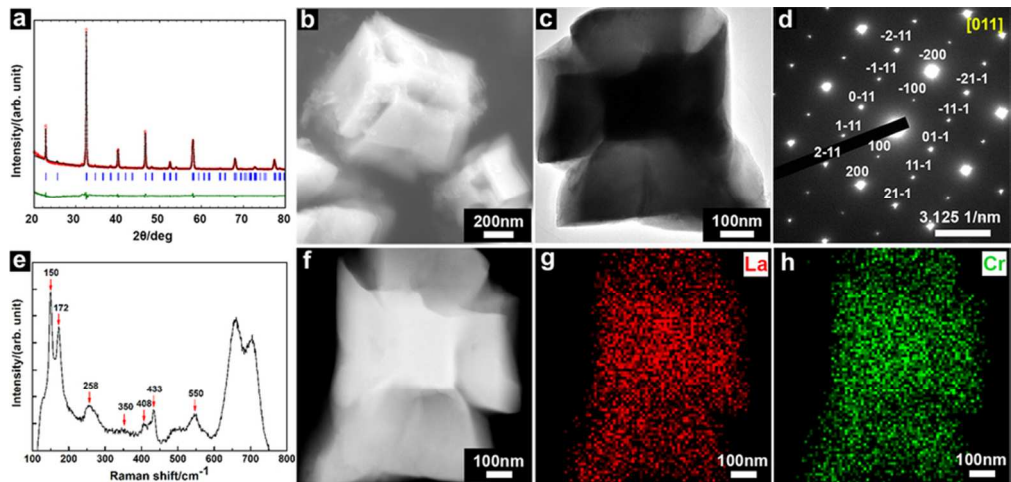
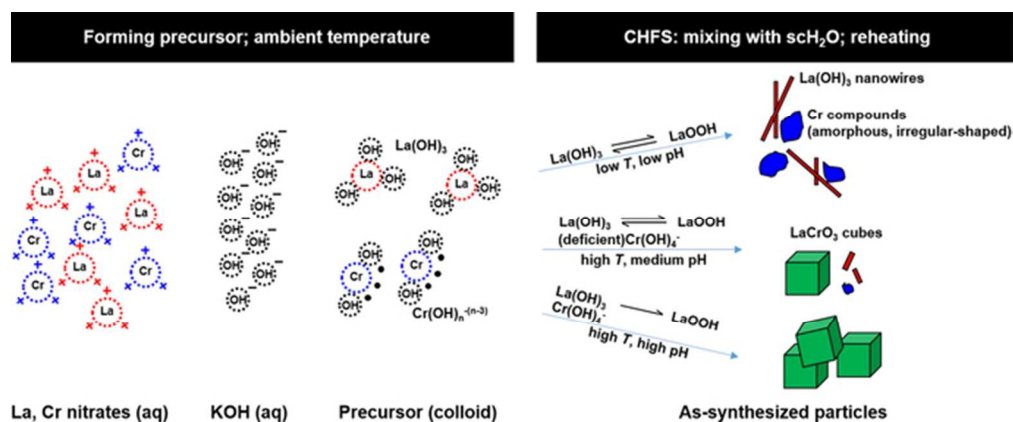


Figure 2. (a) Rietveld refinement of the powder XRD of the LC5 particles; the observed pattern (red circles), the calculated pattern (black line), difference profiles between the observed and the calculated pattern (bottom green line) and the Bragg reflection positions (blue vertical bars) of an orthorhombic LaCrO3 crystal; (b) SEM image of the LC5 particles; (c) BF-TEM image of a LaCrO3 particle; (d) SAED of a LaCrO3 particle; (e) Raman spectrum of the LC5 particles; (f) DF-STEM image of a LaCrO3 particle and STEM-EDS element mapping of the particle, X-ray photons of La La (g) and Cr Ka (h) are presented.

78x37mm (300 x 300 DPI)

Figure 3. Mechanism suggested for the formation of LaCrO<sub>3</sub>.

57x23mm (300 x 300 DPI)

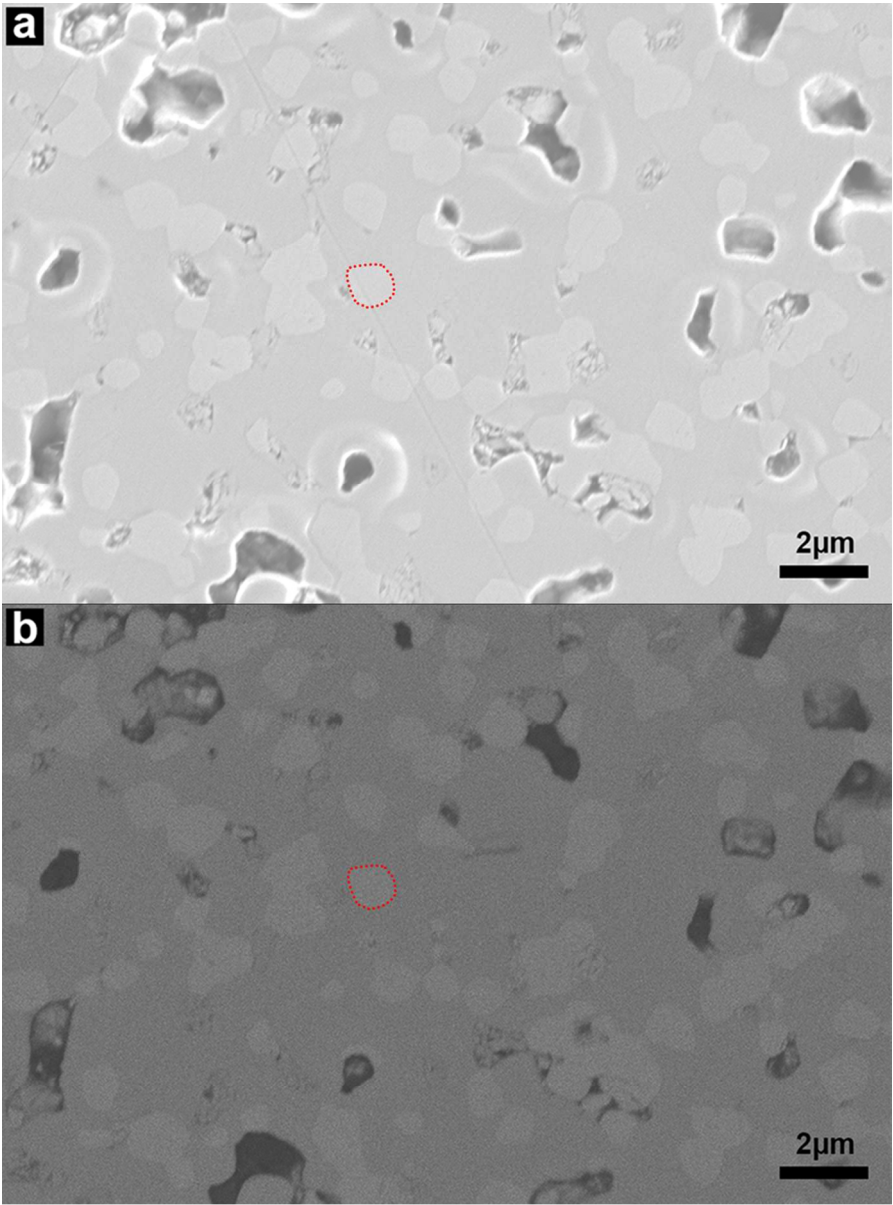


Figure 4. Microstructure of the sintered 10Sc1YSZ – LaCrO3 membranes, presented by HE-SE2 (a) and ES-BSE (b); a LaCrO3 grain is highlighted by red dashed lines.

80x109mm (300 x 300 DPI)

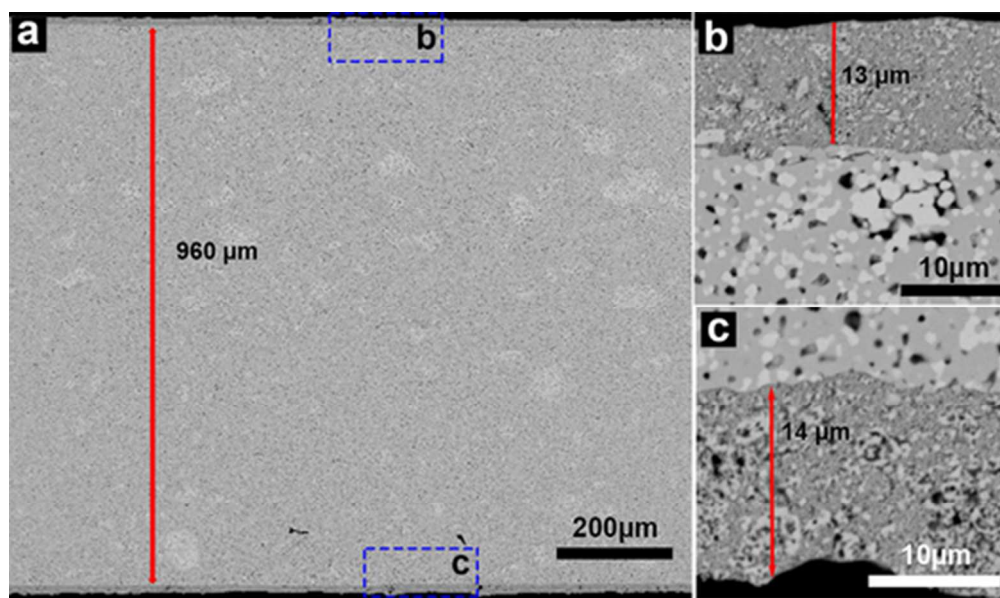


Figure 5. SE2 micrographs of the cross section of the sample for oxygen permeation measurement test.

44x26mm (300 x 300 DPI)



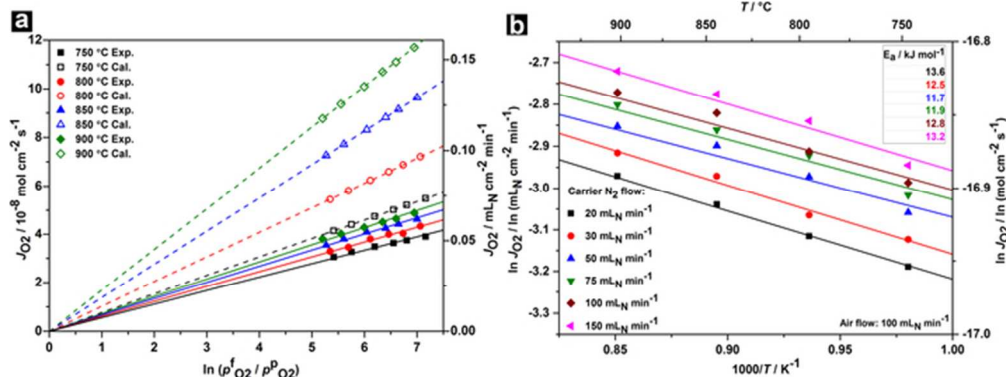


Figure 6. (a) Oxygen permeation flux  $J_{O_2}$  across a 1 mm-thick 10Sc1YSZ – LaCrO3 (65 – 35 vol. %) membrane as a function of the driving force, i.e. log of the ratio between oxygen partial pressures in the feed ( $p_{O_2}^f$ , 0.21 atm) and permeate ( $p_{O_2}^p$ ) side gases. The air flowrate at the feed side was constant at 100  $\text{mL min}^{-1}$ , while  $N_2$  of various flowrates (20, 30, 50, 75, 100 and 150  $\text{mL min}^{-1}$ ) was fed to the inlet of the permeate side. The solid symbols describe the experimental (Exp.) values while the corresponding hollow symbols describe the calculated (Cal.) values. (b) Arrhenius plot of the oxygen permeation flux measured under air. The lines describe the best linear fit to the experimental data.

60x22mm (300 x 300 DPI)